LANGMUIR

pubs.acs.org/Langmuir Article

Spontaneous Formation of Core–Shell Microdroplets during Conventional Coacervate Phase Separation

Chelsea E. R. Edwards, Hongyi Zhang, Ginny Wang, and Matthew E. Helgeson*

Cite This: *Langmuir* 2025, 41, 8510–8523 Read Online

ABSTRACT: We report the single-step formation and stability of protocell-like, core-shell coacervate droplets comprising a polyelectrolyte-rich shell and a solvent-rich vacuole core from the poly(allylamine hydrochloride) (PAH) and poly(acrylic acid) (PAA) system. These double emulsion (DE) coacervate droplets coexist with single emulsion (SE) droplets, suggesting a kinetic mechanism of formation. We use high-throughput microscopy and machine learning to classify droplet morphologies across various final compositions (polyelectrolyte ratios and salt concentrations) and processing routes (mixing rate and thermodynamic path). We find that DE droplets form preferentially over SE droplets at a wide range of compositions using a slow injection mixing rate. DE droplet formation is enhanced at lower salt (NaCl) levels and near 1:1 charge stoichiometry, showing a preference for polycation excess. DE droplets are stable to the micron scale and retain their core-shell structure even after coalescence. Nevertheless, they are metastable; direct observations of various coarsening phenomena suggest that they are primarily stabilized by the viscoelasticity and high viscosity of the polymer-rich shell. Overall, the scalable, simple mixing process used herein offers a novel mechanism to produce multiphase coacervate droplets that is orthogonal to existing routes, which require either dropwise synthesis or thermodynamic tuning.

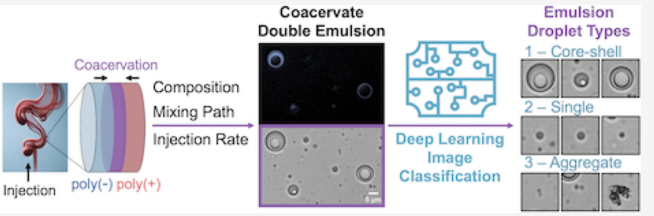

INTRODUCTION

Complexation between oppositely charged macromolecules is prevalent in a broad range of chemistries, including proteins, ionic surfactants, and synthetic polyelectrolytes. As a result, industrial processing of charged functional polymeric materials often involves "coacervation", which occurs when these associations trigger solution phase instability toward liquid-liquid phase separation. Coacervation is common during manufacturing of personal care,[1] food,[2] and other industrial products featuring macroionic ingredients that gel, foam, modify viscosity, or encapsulate. In addition, naturally forming coacervates conduct myriad biological functions in cells as membraneless organelles,[3] like enhancing the rate of biochemical reactions, sequestering inhibitors, and buffering stochastic cellular noise.[4] Across industrial and biological applications, coacervation typically forms a suspension of macroion-dense, single-phase "coacervate" droplets dispersed in a second, macroion-dilute continuous phase.

In more conventional oil-in-water emulsion systems, the development of morphologically complex droplet structures—with multiple subcompartments or phases—has enabled functionalities well beyond what uniform, single-phase droplets could achieve, including applications as delivery vehicles, particle templates, chemical sinks, and more.[5] In coacervate emulsion systems, the need to broaden the diversity of available droplet structures beyond uniform droplets is increasingly relevant, with growing interest in engineering multiphase coacervate droplets for protein encapsulation[6] and drug delivery,[7] and as synthetic bioreactors[8] or lipid-free protocell models for origin-of-life studies.[9] Identifying facile routes to achieve morphologically complex coacervate droplet structures will similarly enable and multiply the engineering possibilities for coacervate emulsions as it has for oil-water emulsion systems.

Two main classes of higher-complexity coacervate droplet structures have been reported to date. The first consists of multiple coexistent coacervate phases that self-organize into a multilayered structure within each droplet. This structure occurs naturally in some membraneless organelles to improve the efficiency of important cellular functions—such as transcription and processing of rRNA[10] and epigenetic inheritance during cell division[11]—by colocalizing the various enzymes, substrates, and reaction products into a given biochemical pathway by preferentially partitioning them into the organelle's successive coacervate layers. In synthetic systems, multilayered coacervate droplets that imitate these organelles have been achieved in a number of biomolecular chemistries, including the associated enzymatic reactions ex

Received: October 22, 2024
Revised: March 7, 2025
Accepted: March 11, 2025
Published: March 25, 2025

https://doi.org/10.1021/acs.langmuir.4c04201
Langmuir 2025, 41, 8510–8523

vivo.[12] These multilayered structures form as a result of mixing multiple coexisting coacervate dense phases, and are stabilized by the careful balance of interfacial tension and macromolecular density between them.[13] In other words, the design rules for multicoacervate multilayer droplets are well-established, yet achieving the desired multilayered droplet structure from these many-component mixtures requires careful molecular design to ensure thermodynamic and interfacial stability.

The second higher-complexity coacervate droplet structure observed to date is the "hollow" or "vacuole-like" structure, in which a dilute watery core is encapsulated within a dense, single-phase coacervate shell. Hollow capsules offer distinct advantages in many broader technological applications, since their interior cavity is particularly useful for carrying a payload and tuning its release.[14] However, as compared to oil-water core-shell emulsion systems, vacuole-like coacervate *droplets* have not been widely demonstrated. Prior works require at least a two-step process to form such structures, reporting their formation after a pre-equilibrated coacervate is exposed to an external change—through the application of an external force, like an electric field[15] or laser tweezers;[16] heating[17−20] or cooling;[21] addition of RNA,[21−23] protein,[24,25] or water;[26] or pH change[17]—that causes it to undergo a phase instability. As a result, much of the work on vacuolated coacervates is more relevant to continuous, porous coacervate matrices than multiphase droplet behavior in single-coacervate systems. While porous coacervate matrices have promising applications—enabling, for example, multimodal release kinetics of a drug in vivo[27]—easily accessing hollow coacervate *droplet* structures would open further possibilities for coacervate-based materials design.

Existing methods to form hollow coacervate droplets—or polyelectrolyte microcapsules—on demand during initial mixing require the use of a templating two-phase emulsion system like PEG/dextran or oil/water, whose interface templates the structure of the coacervate shell that spontaneously forms at the interface.[28] These methods utilize nanoscale interfacial complexation in emulsions (NICE),[29] with one phase containing polycation and the other polyanion, and has been extended to all-water emulsion bodies (AWEsomes) by replacing one of the polyelectrolytes with nanoparticles to improve the shell's mechanical properties.[30] While the resulting structures are broadly promising as nanoengineered microcapsules and protocell systems, they require dropwise addition or microfluidic synthesis to enable reproducible templating of the capsule shape.

There is therefore a need and opportunity to devise more general nonequilibrium routes to form hollow core-shell coacervate emulsions, whereby combinations of fluid mechanics and mass transport during the coacervate bulk phase separation process are used to bias the formation of metastable, vacuole-like droplet structures *en masse*. Methods to increase the complexity of multiphase coacervate droplet structures beyond the *thermodynamics* of multiphase equilibria are currently scarce. By contrast, in oil-water emulsion systems, highly complex multiphase droplet structures are commonly formed in bulk in a single step by tuning the *non*-equilibrium processing path. The effects of shear, pressure drop, and other processing flows on drop formation and destabilization are widely used to control the structure and stability of oil-water droplets.[31] Using a single oil and a single water phase, *kinetically* stable oil-water emulsion droplets with multilayered, cocontinuous, or complex nested structures can be formed through intelligent design of the processing pathway and choosing the right surfactant blend.[5] These advancements suggest that the well-developed literature on multiple oil-water emulsion systems should inspire novel approaches to control droplet structure and functionality in coacervate emulsion systems. For example, we recently demonstrated that colloidal size and aggregation of coacervate droplets could be controlled by tuning the mixing flow conditions used during coacervate formation.[32] Additionally, coacervate droplet coarsening can be suppressed by functionalizing the component polyelectrolytes with a neutral polymer block in either a linear[33] or comb[8] architecture that forms a water-soluble corona around the coacervate core, or by adding dextran to form a polysaccharide layer deposited at the droplet surface,[34] analogous to the role of surfactant in oil-water systems.

Herein, we demonstrate how judicious choice of processing parameters like mixing injection rate can be used to generate a higher-complexity coacervate droplet structure from an emulsion system with a single dense phase. In particular, we discover the spontaneous formation of hollow-core coacervate droplets during bulk mixing, without the need for multiple coexisting coacervate phases or initial multiphase template structures. We characterize this hollow droplet formation over a wide range of preparation conditions—including both composition, mixing paths, and flow effects—and develop a detailed picture of the conditions and mechanisms controlling their formation. Unlike in oil-water systems, the resulting core-shell droplets do not require surfactants to promote their formation, and we propose an evidence-based explanation for their surfactant-free stability. Similar high-complexity droplet structures have not been formed in bulk in a single step from a single coacervate phase until this work.

MATERIALS AND METHODS

Materials. The polycation was poly(allylamine hydrochloride) (PAH), received as dried powder, and the polyanion was poly(acrylic acid sodium salt) (PAA) received as a 35 wt % solution in water from Sigma-Aldrich. Molecular weights of the polymers are reported as M_w = 17,500 g mol^{-1} (degree of polymerization N = 187) for PAH, and M_w = 15,000 g mol^{-1} (N = 160) for PAA. Both polyelectrolytes were used without further purification. Sodium chloride (NaCl, ≥99%) was purchased from Spectrum Chemical and used as received. Milli-Q water was obtained from a Millipore Sigma Simplicity UV system to further purify deionized water (18.2 MΩ ·cm at 25 °C). The dense and dilute phase boundaries for this coacervating system at the same molecular weights used herein have been carefully measured at 1:1 mixing between 0 and 4.5 M NaCl (pH ∼ 7) in our prior work,[35] as well as estimated at nonstoichiometric mixing conditions using a molecularly informed field theoretic model for the PAA/PAH chemistry with N = 150[36] (see ESI Section 1). All compositions tested herein lie within the two-phase region.

Preparation of Stock Solutions. Coacervate emulsions were prepared from mixtures of PAA and PAH stock solutions in Milli-Q with added NaCl. First, concentrated solutions of PAA and PAH were prepared at a 1 M concentration with respect to the number of repeat units, as described in prior work.[32] In addition, a 24.5 wt % solution of NaCl (5 M) was prepared. The final stock solutions were generated immediately prior to each experiment by mixing the appropriate volume of the 1 M polymer and 5 M NaCl solutions into Milli-Q water. Importantly, we found no evidence of salting-out or self-assembly of either polymer prior to mixing, as in prior work.[32]

Mixing Procedures. A variety of PAA/PAH solution volume ratios, injection rates, and compositions were used herein, as the mixing procedure was found to significantly affect core-shell DE droplet formation. Different variables are held constant during

https://doi.org/10.1021/acs.langmuir.4c04201
Langmuir 2025, 41, 8510−8523

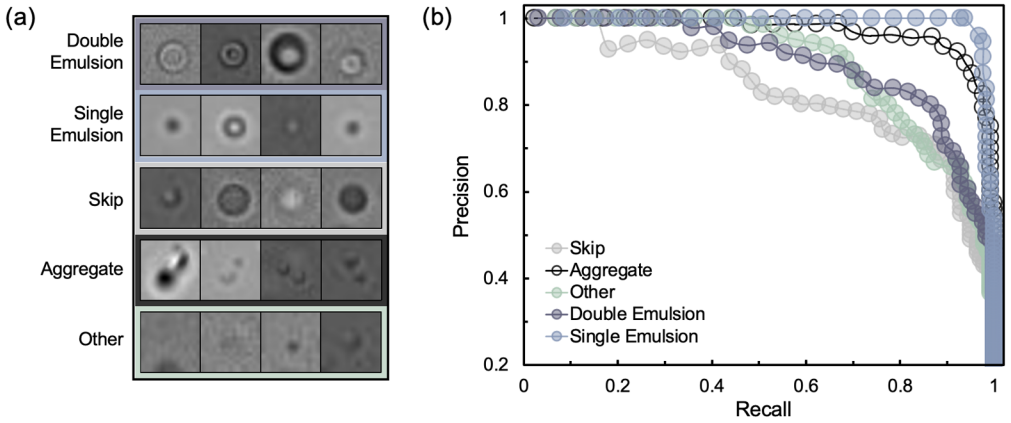

Figure 1. Summary of machine learning model for identifying droplet morphologies. (a) Typical ROI corresponding to each droplet category. Scale varies; $r \approx 1$ μm for a typical droplet (pixel size is 0.293 μm/pixel). (b) Precision-recall curves for each droplet category, evaluated using the test set, show the trade-off between the model's ability to find the droplets in a given category (recall) versus its ability to accurately identify the category of droplets (precision). An ideal model has area under the curve (AUC) = 1.

different mixing procedures. To avoid ambiguity, we provide all details for each mixing procedure alongside the resulting data set in the subsections of "Mixing Conditions Favoring Double Emulsion Formation" in the Results and Discussion, where these concepts are introduced. In "Composition", the final composition is varied while the injection rate and volume and composition of the mixed stock solutions are held constant during mixing. In "Mixing Speed", the injection rate is varied while the final composition, composition of the mixed stock solutions, and injection volume are held constant during mixing. Finally, in "Salt Gradient", the composition of the mixed stock solutions is varied, while the injection rate, volume, and final composition are held constant.

Automated Imaging. Micrographs were collected using an Axio Observer 7 microscope outfitted with a computer-controlled motorized sample stage and motorized autofocus objectives, and recorded with an Axiocam 702 monochromatic camera under brightfield illumination. The study employed a motorized 20× autofocus air objective with a numerical aperture (NA) of 0.6, corresponding to a pixel size of 0.293 μm. The environmental chamber maintained a controlled temperature of 25 °C. Automated imaging experiments were conducted as follows. Samples were mixed as described in the subsequent sections, with $t = 0$ taken to be the second at which mixing was completed. 100 μL of sample was transferred to a glass-bottomed 96-well plate, which was loaded into the Zeiss microscope. Autofocus was preset to a fixed distance of ∼1 to 5 μm above the glass surface. The microscope was preprogrammed to acquire 8, nonoverlapping brightfield images spanning the well area. Exposure time was optimized prior to imaging each sample using the automatic settings provided by the Zeiss software. To provide a reliable comparison between different mixtures given the metastability of the DEs—as well as to prevent the effects of aging (such as core expulsion) from affecting comparisons between DE formation propensity at various mixing conditions and compositions—automated imaging was conducted at precisely 3 min after mixing completed for each sample.

The image series and corresponding videos used to study destabilization mechanisms were captured manually rather than automatically, and the destabilization mechanisms were generally observed and captured well past 3 min after mixing. However, these image data otherwise utilized identical microscope, objective, camera, and other parameters just described.

Image Processing. *Trajectories.* To track the cores and shells of double emulsion (DE) droplets as a function of time, a custom MATLAB code was generated. Conventional multiple particle tracking algorithms (i.e., Crocker & Grier) identify nonoverlapping spheres,[37] and thus were not possible for the images herein. In each video frame, the imfindcircles function was used to find both the outer and inner radii. The outer radius was detected by specifying a size between 5 and 100 pixels, and the inner by specifying a dark object polarity and size between 3 and 8 pixels. The predicted inner and outer sizes deviated across frames by only 1.7 and 5.8%, respectively. Examples of the inner and outer radii fit circles overlaid on top of core-shell micrographs are provided in Figure S1.

Droplet Classification. An image classification machine learning (ML) algorithm was used to differentiate the core-shell "double emulsion" (DE) structures from conventional "single emulsion" (SE) droplets within the same image and across compositions. In addition, the algorithm differentiated DE and SE droplets from those that were not clearly in either category—namely, overlapping or droplet structures and out of focus droplets—as well as background noise.

Model Development. The model required a well-labeled set of images in each category for training. Prior to categorization by ML or for the training data set, regions of interest (ROI) were identified and cropped from images using a custom Python code described in ESI Section 3.2. To create the training data set, we manually sorted ROI into five categories. Double-emulsion or "DE" droplets had an obvious core-shell structure. Single emulsion or "SE" droplets were single dots of black or white surrounded by background. ROI containing multiple or overlapping droplets, or otherwise irregular shapes (e.g., dust particles), were labeled as aggregate or "Agg" structures. The "Skip" category differentiated droplets that could not be clearly distinguished as a core-shell, i.e., droplets with possible irresolvable substructure typically due to being out-of-focus or very small. Finally, the "Other" category described background noise or ROI that only captured the edge of a droplet. Example droplets from each category are illustrated in Figure 1a, with more examples of each provided in Figure S2. The inclusion of Agg, Skip, and Other labels significantly enhanced the model's ability to correctly detect and differentiate well-defined, in-focus DE and SE droplet structures.

To learn the model, the 4142 training ROI and their associated labels—SE, DE, Agg, Skip, or Other—were archived into a database. Data augmentation to obtain 13,400 total labeled ROI (2680 per type) is described in ESI Section 3.4. The total data set was split randomly into a training set learned by the ML model (95%, or 12730 labeled images) and a test set used to evaluate the ML model's accuracy after training (5%, or 670 labeled images).

The model was trained using the Google Colabs platform with the AutoGluon (version 0.8.2) multimodal ML package (AutoMM) using MultiModalPredictor in Python (Pytorch version 1.31.1 + cu117). We used a convoluted neural network (CNN) model with 12 hidden layers. Accuracy was used as the validation metric. The activation function was a Rectified Linear Unit (ReLu) and the loss function was the categorical cross-entropy model. The ML model was trained over 10 epochs, with 899 global steps total. During the training process, the model was evaluated on the validation set after every 45 global steps (twice per epoch). Justification and further explanation of these

https://doi.org/10.1021/acs.langmuir.4c04201
Langmuir 2025, 41, 8510−8523

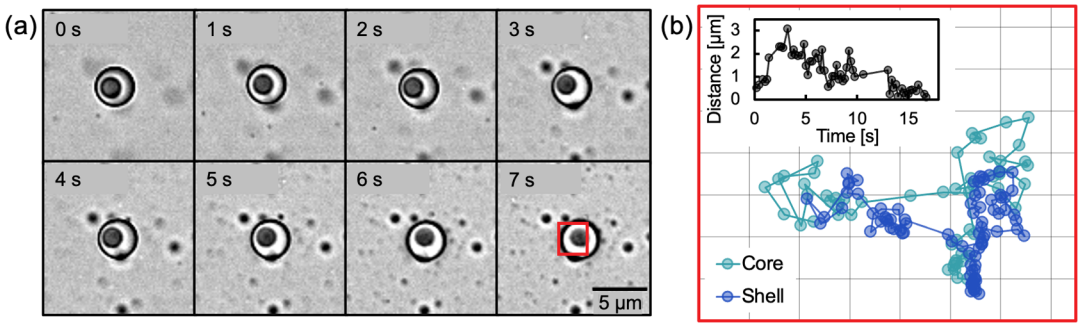

Figure 2. A typical core-shell droplet structure from mixed solutions of PAA and PAH in water is tracked using video imaging. (a) Brightfield micrographs of the core-shell coacervate droplet sedimenting onto a glass slide. (b) Trajectories of the droplet's core and shell centers are individually monitored, illustrating distinct yet interrelated Brownian motion patterns. Axes represent the distance (pixels) from the center of the micrographs, corresponding to the red square outlined in (a). Inset shows the time progression of the real distance between core and shell centers. Composition: 30 mM with respect to the number of PAA and PAH repeat units (r.u.), 1:50 mol:mol PAH:PAA, 2.5 M NaCl.

selections and functions is provided in ESI Section 3.5. The model achieved a validation accuracy between 83.7 and 84.1% in the top 3 evaluations during the training process. These three checkpoints were subsequently fused via the greedy soup algorithm to create the final model.

Model Performance. The classification ML model was determined to have an 83.9% overall accuracy according to its performance on the validation set during model training. The model's ability to accurately and precisely categorize droplets in the test set reveal its detailed performance abilities for each droplet type. Confusion matrices describing the trained model's predictions for each category relative to the true labels are available in Table S1 expressed as a percentage, and numerically in Table S2. The model was able to predict between 72 and ~95% of the labels correctly across all categories in the test set. Categorized by type, accuracy is 98.2% for single-phase emulsion droplets (SE); 92.5% for core-shell or double-emulsion droplets (DE); 89.6% for out of focus droplets (Skip); 97% for overlapping or multiple droplets in a single ROI (Agg); and 90.4% for background noise or artifacts (Other). As a point of reference, a recent survey on deep learning algorithms in microscopy image analysis identified 12 published image classification studies—all for cell classification (e.g., detection of cancerous cells)—whose accuracies (Jaccard index) averaged 90.5% with a standard deviation of 10.0%, ranging from 66 to 99.5%.[38]

The precision-recall curve evaluated using our trained ML model with the test set is shown in Figure 1b. The area under the curve (AUC) metric calculated from this curve can provide insights as to how well the model can identify DEs among the other droplet types while maintaining a high level of precision. A perfect AUC value is 1.0, and 0.5 is prediction equivalent to random chance. The calculated AUC values are 0.970 for SE, 0.884 for DE, 0.961 for Agg, 0.822 for Skip, and 0.877 for Other. Thus, our model exhibits exceptional proficiency in recognizing and distinguishing SEs and aggregates, and it performs quite well at distinguishing DEs and mitigating noise into the Other category. More detail about calculation and interpretation of the precision-recall curve and AUC is available in ESI Section 3.6. Other performance metrics—namely the true positive (TP) and false positive (FP) rates; true negative and false negative (FN) rates; positive and negative predictive values; and the false discovery rate—and the raw numerical values of true and false positives and negatives for each category are provided in Table S3.

Model Workflow. To run the trained ML model on test image data, the model and micrograph to be labeled are loaded into a Google Colabs workspace. ROIs are identified in the micrograph as described in ESI Section 3.2. Typically between 1000 and 5000 ROI are detected per micrograph depending on the composition. Each ROI is evaluated and labeled using the trained model. To avoid double-counting, we reject any ROI fully contained within another larger ROI. Label counts are summed to return the final statistics for each droplet type.

RESULTS AND DISCUSSION

Two-Polyelectrolyte Core-Shell Droplets. Double-emulsion (DE) droplets, characterized by a core-shell morphology, are formed from mixed solutions of PAA and PAH upon initial mixing. A time-lapse sequence of one such core-shell droplet sedimenting onto a glass slide is shown in Figure 2a. This novel droplet structure comprising three phases from only two polyelectrolyte components often coexists with the well-studied classical single-emulsion (SE) droplets also formed by the PAA/PAH system,[32,39] with relative propensity to form each morphology dependent on mixing ratios and conditions detailed in the following subsection.

The individual Brownian motions of the shell and core of this droplet are tracked in Figure 2b. The trajectories of the centers of the core and shell are clearly coupled, but their relative motion illustrates that the core is mobile within the droplet; the shell retains fluid-like properties. Tracking methodology is described in "Image Processing" in Materials and Methods.

Fluorescence microscopy aided by autofluorescence of the polyelectrolytes was used to verify the two-phase morphology of the DE droplets (Figure 3). The intrinsic fluorescence of PAA/PAH coacervates has been used previously to image vacuoles in a continuous coacervate matrix. It is also observed in individual powders and solutions of PAA and PAH, and may

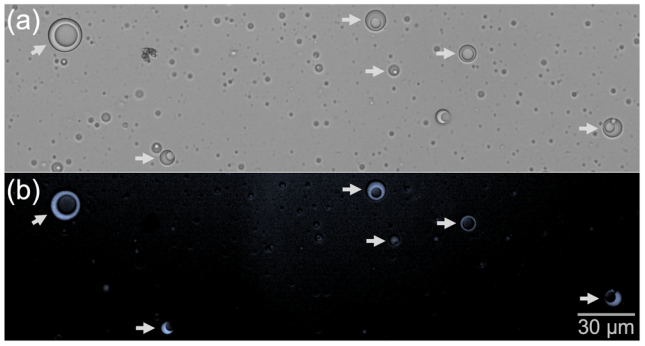

Figure 3. Fluorescence microscopy verifies that the double emulsion droplets have polyelectrolyte-dense shells and dilute cores. (a) Brightfield and (b) fluorescence micrograph (ex: G365 nm, em: BP 445/40; contrast is enhanced). Weak autofluorescence of the concentrated polyelectrolytes reveals that the core of the droplets are dilute. The total solution contains 30 mM r.u., 50:1 mol:mol PAH:PAA monomer at 2.5 M NaCl.

https://doi.org/10.1021/acs.langmuir.4c04201
Langmuir 2025, 41, 8510−8523

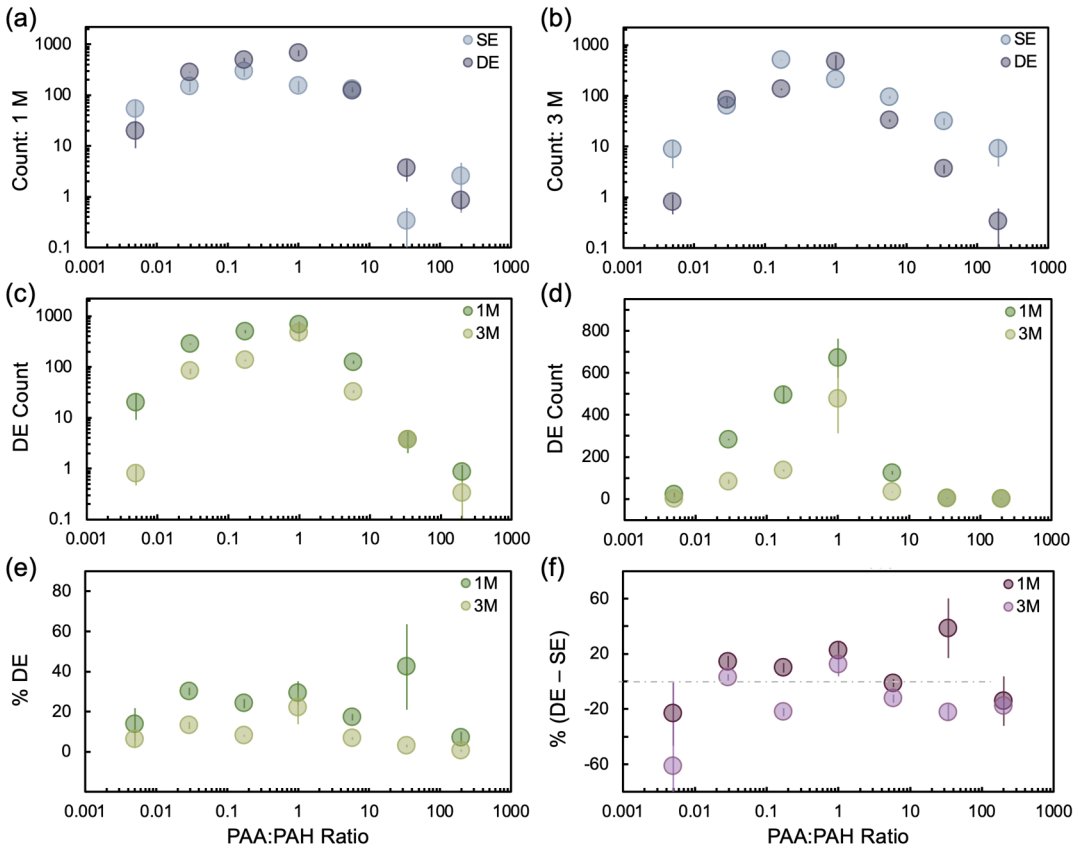

Figure 4. Formation propensity of single and double emulsion droplets at various PAA:PAH ratios and at low vs. high salt. Average counts of SE vs. DE droplets per microscopy image (counts/0.200 mm^2 area) are shown at (a) 1 M NaCl and (b) 3 M NaCl. (c) Comparison of the DE count at 1 vs. 3 M NaCl in log scale and (d) linear scale. (e) The prevalence of DE on average at each salt condition, expressed as a percentage of the total number of droplets in the system (accounting for SE, DE, Agg, and Skip). (f) The average prevalence of DE droplets relative to SE droplets is expressed as a percent difference of the total number of droplets in the system (accounting for SE, DE, Agg, and Skip). Negative values of this difference (below the dotted line) form fewer DEs than SEs at that condition, with larger magnitude reflecting a greater difference in formation propensity. DE are less favored farther from 1:1 stoichiometry. Error bars indicate standard error ($n \geq 3$).

originate from initiator residue.[26] Autofluorescence imaging is preferable to labeling the dense phase with a (typically bulky and hydrophobic) fluorescent dye, since prior work has demonstrated that the presence of hydrophobic domains[17] or aliphatic groups (e.g., fatty acids[40]) can result in heterogeneous or multiphase coacervate structures. In Figure 3b, the dark core thus corresponds to the polyelectrolyte-dilute phase, and the fluorescent shell corresponds to the polyelectrolyte-rich dense phase. Hollow core-shell coacervate droplets have not previously been observed in the solution phase, i.e., as a spontaneous emulsion. Rather, in prior works, vacuoles within the dense phase or within sedimented coacervate droplets have been induced through changes in external parameters such as temperature[12,20] or composition,[21,24] or grown within the dense phase as a result of coacervate aging,[21,32] after local equilibration of the dense and dilute phases into a single emulsion.

The "hollow" core-shell DE droplets formed herein contrast with the majority of multiple emulsion coacervate droplets reported in the literature, which consist of multiple mixed dense phases (i.e., where both the core and shell are coacervates). In the present PAA/PAH system, experiments using symmetric polyelectrolytes have observed a single dense phase, so theories describing complexation[41,42] and a recent molecularly informed field theoretic model for the PAA/PAH coacervating system[36] have been developed accordingly. Under the ideal assumptions of a two-macroion system of symmetric polyelectrolytes (both of similar molecular weight and charge fraction) and monovalent counterions of the same size, the concentrations of polyanion/polycation and small anion/cation are equivalent; such a mixture is essentially a two-component system due to local electroneutrality.[41] However, in the real system, the polyelectrolytes are not perfectly symmetric: therefore, by the Gibbs Phase Rule, even the PAA/PAH and NaCl system—consisting of a single polyanion and polycation species with counterions in water—could form multiple condensed or multiple dilute phases. This may be one possible explanation for our observation of hollow coacervate droplets. However, our DE droplets do not necessarily comprise equilibrium phases, as explored below.

Mixing Conditions Favoring Double Emulsion Formation. As evident in the micrographs of Figure 3, only a fraction of the droplets exhibit a core-shell double emulsion (DE) droplet structure, with the rest comprising a single-emulsion (SE) structures, i.e., they do not contain a dilute core. This indicates that DE droplets are not equilibrium structures, and that their formation and stability compete with that of SE droplets. This Section evaluates the formation propensity of the core-shell DE structure in order to identify processing and compositional conditions that promote the formation of DE droplets. Specifically, we investigate how the mixing conditions—composition, mixing rate, and thermody-

https://doi.org/10.1021/acs.langmuir.4c04201
Langmuir 2025, 41, 8510−8523

namic mixing path—affect the tendency to form core-shell DE droplets relative to SE droplets, and suggest guidelines for choosing these parameters in order to enhance core-shell formation.

Composition. To investigate how the composition of the final PAA/PAH mixture affects formation of DE structures, we examined emulsion formation in solutions mixed at a wide range of PAA:PAH ratios. Mixing was conducted by preparing stock solutions of PAA and PAH at total polyelectrolyte and salt (NaCl) concentrations equivalent to that of the final mixture. The total mixed polyelectrolyte concentration was fixed at 20 mM with respect to the number of repeat units (r.u.). Prior works on the PAA−PAH system of the same molecular weights and comparable composition[32,35,43] found that variations in r.u. have a comparatively small effect on the properties of the resulting coacervate, particularly when compared to changing salt concentration. Here, NaCl concentration was varied between 1 and 3 M. The salt-free condition is unreported, since we could not obtain reliable counts across PAA:PAH ratios with our current methods due to higher droplet concentrations and large prevalence of droplet aggregates like those observed in prior work.[32]

With this approach, different PAA:PAH ratios were obtained by varying the relative volumes of the two stock solutions. To ensure equivalent fluid dynamics of mixing across different compositions, the volume of the charge stoichiometry-limiting polyelectrolyte stock was fixed at 1 mL, and added over a duration of exactly 1 s by pipet injection into the stock of excess polyelectrolyte. Each mixture was capped in a 5 mL tube, inverted twice, then 100 μL of sample was transferred into a 96-well plate for automated microscopy (see "Automated Imaging" in Materials and Methods). Images were captured at precisely 3 min after mixing to minimize the effects of droplet spreading and other destabilization mechanisms. The resulting micrographs were analyzed to count the number of SE and DE droplets in each image using a custom machine learning algorithm (see "Droplet Classification" in Materials and Methods). The following results report average "counts" per image (size 0.200 mm^2: 562.56 μm × 356.29 μm), with error bars reflecting the standard deviation of counts between different micrographs.

Figure 4a,b report the prevalence of DE and SE droplet structures across various mixing ratios of PAA:PAH at low (1 M) and high (3 M) NaCl concentrations. Under both salt conditions, proximity to the 1:1 mixing condition favors the formation of the highest quantities of both SE and DE droplets. Note that the *y*-axis is plotted on a logarithmic scale, so the differences in absolute values between formation of droplets nearer the 1:1 mixing case and nearer 1:100 or 100:1 mixing differs by 1−2 orders of magnitude. The counts at these 1 and 3 M salt conditions for all droplet types—i.e., including droplets classified into the aggregate and skip categories—are provided in Figure S3.

Formation of conventional single-emulsion coacervate droplets is favored under polycation excess (PAA:PAH < 1) as compared to the reciprocal ratio with polyanion excess. The observation that the volume fraction of the dense phase—the dispersed phase in the emulsion—is higher under PAH excess is consistent with recent molecularly informed field theoretic simulations on the PAA/PAH system that predict a broader phase separation boundary (i.e., higher propensity to form coacervates) in the PAH-excess case.[36] The propensity to form double emulsion droplets also follows this trend, consistent with the hypothesis that the prevalence of both single and double emulsion droplets depends on the overall thermodynamic driving force for coacervation.

Next, we explicitly compare DE formation in solutions with low (1 M) vs. high (3 M) NaCl concentrations. Figure 4c,d show DE counts at various PAA:PAH ratios in logarithmic and linear scales, respectively. Broadly, these comparisons demonstrate that more DEs form at low salt conditions across every PAA:PAH mixing ratio. Since coacervation is critically dependent on the electrostatic strength, conditions with lower salt concentration/higher electrostatic strength correspond to state points deeper into the two-phase region, resulting in a larger theoretical dense-phase volume fraction at equilibrium. Thus,

the greater propensity to form DE at lower vs. higher added salt is again consistent with an increased thermodynamic driving force to form coacervates in general. Note that under conditions of polycation excess (PAA:PAH < 1), the difference between low-salt (1 M) vs. high-salt (3 M) DE count is increased relative to the corresponding condition with polyanion excess. This difference is shown explicitly as a function of PAA:PAH ratio in Figure S4.

However, thermodynamic considerations do not necessarily inform the relative propensity of core-shell DE droplets—either as a fraction of the total droplets formed or compared to the prevalence of unstructured SE droplets—at a given composition. Therefore, to understand how composition affects DE formation relative to the formation of SE droplets, we calculate the percentage propensity of DE droplets, using the sum of SE, DE, aggregated, and skipped counts to determine the total number of droplets formed at each condition (Figure 4e). This reveals that low salt (1 M) enhances core-shell droplet formation relative to the total number of droplets formed, as compared to high salt (3 M), at every PAA:PAH mixing ratio. Our rationale for the observed enhancement of core-shell droplet formation at low salt and under polycation excess is presented and supported by additional observations discussed below in "Surfactant-Free Stabilization of Coacervate Double Emulsion".

In Figure 4f, the relative abundance of DE droplets is expressed as the average percent difference between SE vs. DE droplet formation at various PAA:PAH ratios. Positive values of this difference indicate that DEs are enriched relative to SEs at that condition, and vice versa for negative values. Thus, conditions where this percentage is most positive are those for which formation of core-shell droplets is most strongly favored relative to formation of other droplet types. This comparison reveals that the propensity to form core-shell DE droplets relative to unstructured ones is enhanced nearer the 1:1 mixing condition (more negative values at both salt conditions). Conditions further from stoichiometric mixing and with higher salt concentration, are more likely to form unstructured emulsions rather than core-shell double emulsions.

When considering the relative number of DE droplets compared to the total number of droplets in the system in Figure 4e,f, the enhancement in DE formation under excess PAH versus under excess PAA disappears. It is still helpful to know that a greater number of DEs are formed under polycation excess, as observed in Figure 4a−d. However, taken together, these observations suggest that the greater number of core-shell droplets formed under polycation excess is simply a consequence of the greater number of total droplets generated,

https://doi.org/10.1021/acs.langmuir.4c04201
Langmuir 2025, 41, 8510−8523

rather than the core-shell DE droplet structure *itself* being favored relative to other droplet structure types.

Mixing Speed. In oil-water double emulsion systems, it is common for the physical aspects of the mixing process such as the shear rate or mixing energy to affect the final morphology formed during the emulsification.[5] In the case of the coacervate multiple emulsions herein—which form spontaneously during initial mixing without the need for additional shear steps or inducing a phase separation after formation of the coacervate—the primary parameter of the mixing flow that may affect DE formation is the rate of injection during which the solutions are initially mixed. This time scale sets the shear rates for mixing as well as the length scale for any recirculating laminar eddys or flow structures that form under confinement in laminar injection.[44] Decreasing the injection time (faster injection) is analogous to increasing the Reynolds number (*Re*) during the mixing, via faster fluid flow rate. It also increases momentum transfer by increasing advection, as well as the role of eddys. These effects also result in an increased Schmidt number (*Sc*, the ratio of momentum to mass transfer rate) and Peclet number (*Pe*, the ratio of advective to diffusive transport rates) accompanying faster injections.

Since high-shear rate processing is often used to form water-in-oil-in-water (W/O/W) double emulsions, one might naïvely expect a faster mixing speed (shorter injection time) to produce a greater number of DE droplets than SE droplets for the same composition. Instead, we observe the opposite trend for our coacervate double emulsions. To demonstrate this, the same mixed final composition was prepared by varying the injection *time* of the limiting-polycation stock, enabling variation of the mixing mechanics. In particular, the final mixed solution composition was 2.5 M NaCl and ≈30 mM polyelectrolyte (50:1 PAA:PAH) in Milli-Q water with a final volume of 1 mL, with two distinct pairs of PAA and PAH stock solutions—compositions A and B—represent different mixing paths employed to generate this final composition (details provided in ESI Section 4.2). Figure 5 illustrates that, for a fixed mixing path, increased injection rates suppress core-shell formation. In addition, while the abundance of core-shell structures is modulated by the injection rate, the number of single emulsion droplets formed remains about the same (SE, DE, Skip, and Agg counts at all injection rates for compositions A and B are provided in Figure S5). Thus, as injection rate increases, core-shell droplets make up a progressively smaller proportion of total droplet structures relative to SE, from around 1.2−0.01% in composition A and from around 7.5−0.2% in composition B (Figure 5). The percent difference (SE−DE) increases from around 59−83% in composition B and from around 90−99% in composition A. From this, we conclude that slow, gentle mixing best favors core-shell DE formation for a fixed thermodynamic mixing path.

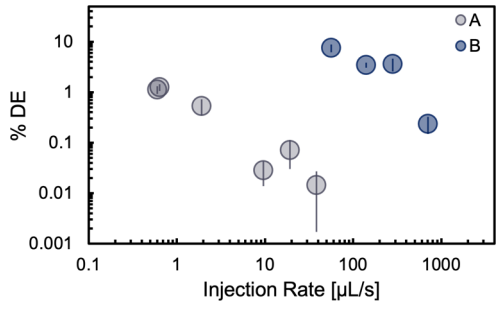

Figure 5. Injection rate strongly controls DE formation propensity. The prevalence of DE at each salt condition is expressed as a percentage of the total number of droplets in the system (accounting for SE, DE, Agg, and Skip). Error bars indicate standard error ($n \geq 3$). Compositions A and B represent two distinct pairs of PAA and PAH stock solutions which were mixed to generate coacervates at the same final composition of 2.5 M NaCl and ≈30 mM polyelectrolyte (50:1 PAA:PAH) in Milli-Q water (details provided in ESI Section 4.2).

While the results in this section utilize a nonstoichiometric PAA:PAH ratio, the stoichiometric PAA/PAH andNaCl system has been well-studied in prior work by us and others.[32,35,39] These studies neither varied injection mixing rate nor observed a significant presence of core-shell droplets. Whereas, herein we observe a large prevalence of core-shell droplets at the 1:1 stoichiometry (Figure 4) by using an intentionally slow injection rate inspired by the results shown in Figure 5. Thus, we suspect that the suppression of core-shell formation with fast injection rate is generalizable across PAA:PAH ratios, though we leave direct quantification of this effect across all compositions to future work.

In addition, the results in this section suggest that a core-shell droplet morphology might be achieved in a wider variety of classical coacervate chemistries beyond the PAA−PAH system, simply by using a slow injection rate to mix the polyelectrolyte components. Determining which aspects of the polyelectrolyte chemistry enable formation of spontaneous core-shell droplets during mixing would be a promising area for future study. The potential generality of the core-shell formation mechanism proposed herein is discussed in detail below in "Formation Mechanism".

Salt Gradient. Another variable that may affect formation of the DEs is the compositional gradient across the two mixing streams. As discussed above, the rheology of the dense coacervate phase is highly sensitive to the salt concentration, and so here we chose to examine the effect of the salt concentration gradient between the two mixing streams. Specifically, we varied the difference in salt content between the two stock solutions being mixed while fixing the final composition and injection rate. This is feasible in cases of highly off-stoichiometric mixing, where changing the salt concentration in the limiting solution over a wide range of conditions minimally affects the final salt concentration after mixing. The final mixed solution composition contained 30 mM polyelectrolyte (50:1 PAA:PAH) and averaged 2.472 M NaCl (0.6% variation across mixtures) in Milli-Q water with a final volume of 1 mL. The injection rate was ≈9.6 μL/s. Here, we report results as a function of the "salt difference," which we define as the difference in NaCl molarity between the polycation (PAH) and the polyanion (PAA) solutions used for mixing. The exact compositions of PAA and PAH stocks as well as the final mixed compositions used in this section are listed in Table S4.

The salt content of a stock solution affects the solvent quality and molecular conformation, ion adsorption, and water structure around polyelectrolytes.[45] Salt changes the phase diagram and rheology of the PAA/PAH coacervates,[35] and also affects the diffusivity and viscosity of polyelectrolytes in the individual stock solutions.[45] Any of these effects could play a role in DE formation. In particular, varying the salt difference of the stock solutions will impact the mass transport kinetics with respect to the phase separation process during mixing.

Overall, we observe a weak trend in the effect of salt difference on the DE formation propensity (Figure 6). At

https://doi.org/10.1021/acs.langmuir.4c04201
Langmuir 2025, 41, 8510−8523

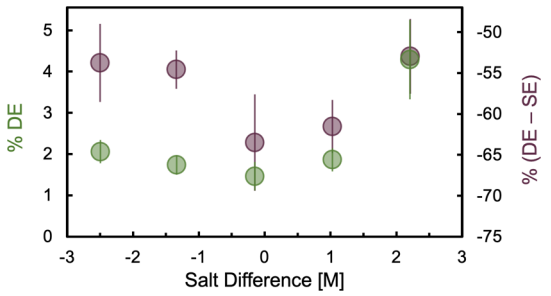

Figure 6. Percentage of total droplets exhibiting a core-shell (DE) structure (green) and the percentage of DEs relative to single emulsion (SE) droplets (purple) are shown as a function of the difference in salt content between the mixed polycation and polycation stock solutions. Final composition and injection time (1 s) remain fixed; final NaCl concentration varies by 0.6%. More negative values of the percentage difference (purple) reflect less formation of DEs relative to SEs. Thus, mixing at a greater salt difference slightly enhances relative DE formation (p = 0.05). Error bars indicate standard error ($n \geq 7$).

smaller magnitude of the salt concentration gradient, we observe slightly suppressed formation of the double emulsions relative to mixing at larger salt gradients (p = 0.05). This weak trend is expressed both as a percentage of the total number of droplets that are core-shell, and as a percent difference relative to the percentage of single emulsion droplets. Generally, *fewer* DE droplets form relative to their SE counterparts when the polycation and polycation solutions are mixed at similar salt concentrations. The total counts of each droplet category at each salt difference (SE, DE, Skip, and Agg) and a box plot showing all individual percent difference values corresponding to the reported standard errors are provided in Figure S6.

To summarize, we generally observe that a *smaller* fraction of DE droplets form when the polycation and polyanion solutions are mixed at similar salt concentrations, rather than across a salt gradient. There could be multiple reasons for this weak effect, including solvent quality and differences in viscosity between the solutions.

Surfactant-Free Stabilization of Coacervate Double Emulsion. In conventional oil-water double emulsion (DE) systems, interfacial stabilization of multiple emulsion droplets is commonly achieved by using surfactant blends, in which surfactants with different relative sizes of the oily and hydrophilic moieties (i.e., different hydrophile−lipophile balance or HLB values), can preferentially stabilize the inner and outer surfaces of the droplet shell according to the geometry of the surfactant relative to the local radius of curvature and directionality of the interface.[5] In conventional coacervate single emulsion (SE) systems, amphiphilic moieties like small-molecule fatty acids,[40] lipids,[46] and proteins,[47] have all been shown to localize at the interface between coacervate and dilute phases. Recent reports on systems of hollow protein droplets have additionally postulated that the adsorption and "liquid crystalline-like" ordering of amphiphilic protein segments at both the inner and outer interfaces of the core-shell droplet are responsible for their stability.[17,23] However, in the PAA/PAH DE system herein, neither was surfactant added, nor other moieties introduced to reduce the interfacial tension. Therefore, it is initially unclear how to conceptualize the stabilization of these DE droplets, since the previously described mechanisms of interfacial stabilization are unavailable. The stability of our observed DE structures likely arises from a different mechanism, which we investigate in this section.

Here, we probed the origin of stability of the core-shell coacervate droplets by making direct observations of their *in*stability mechanisms using optical microscopy. In Figure 7a, we demonstrate that the coacervate DEs coarsen primarily by coalescence of the shells. This is a characteristic coarsening mechanism for all-liquid emulsions and is predominant in classical single emulsion coacervate systems,[48] as first observed by Bungenberg de Jong in 1949.[49] Importantly, the ability to coalesce suggests that the coacervate remains liquid-like,[13] since gel-like coacervates resist coalescence.[50] This inference is consistent with the liquid-dominant equilibrium rheology of the PAA/PAH system at stoichiometric mixing of the homopolyelectrolytes with the same chain lengths and region of composition space studied herein, as has been characterized in prior work.[35,43]

In Figure 7b, we observe two dilute phase droplets within a larger dense-phase droplet coalesce to form a single dilute core. This coalescence event takes significantly longer than the external coalescence of shells in Figure 7a, since time scales governing the initial coalescence event and relaxation afterward are slowed by the high viscosity of the intervening dense coacervate phase, which is orders of magnitude higher than the dilute phase.[35] In particular, the coalescence of shells in Figure 7a occurs as soon as the two droplets become proximate. By

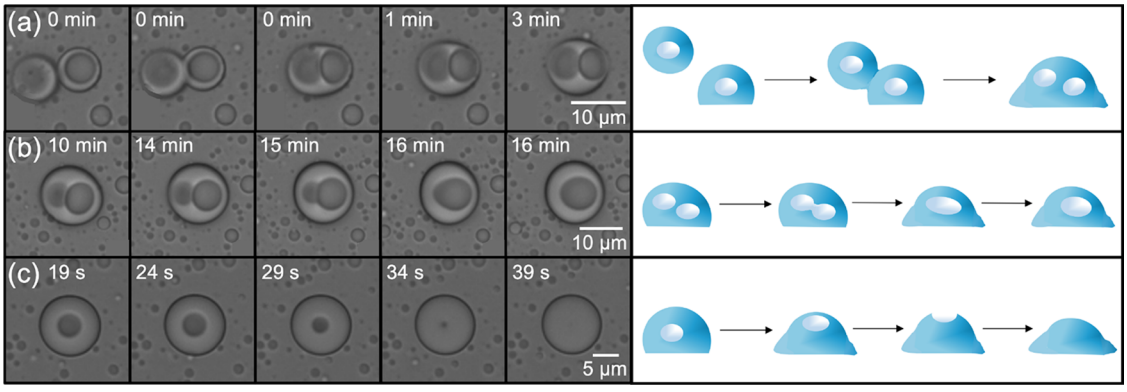

Figure 7. Destabilization mechanisms of DE coacervate droplets. (a) Coalescence of the shells of two DE droplets. (b) Coalescence between two dilute cores within the same droplet. (c) Escape of the dilute core occurs as a sedimented DE droplet spreads onto the glass slide, recovering a uniform droplet structure.

https://doi.org/10.1021/acs.langmuir.4c04201
Langmuir 2025, 41, 8510−8523

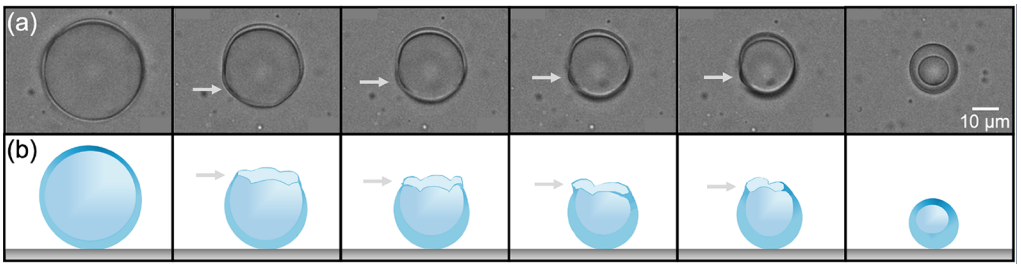

Figure 8. In larger DE droplets, the dilute core can be partially retained during core escape. (a) Time-lapse micrograph of a large DE droplet ($\frac{r_{drop}}{r_{core}} \approx 1$) shows a flowering-like mechanical instability in the shell's response at the rim of the rupturing interface. The final structure retains a dilute core. (b) Schematic of the core escape in (a), indicating the observed mechanical instability at the rim during the bursting event.

contrast, the cores in Figure 7b neighbor one another for several minutes within the larger droplet prior to coalescence, due to the high viscosity of the intervening coacervate phase. A video of shell and core coalescence is available in ESI Video 1. Coarsening of the cores can also occur by Ostwald ripening, as seen in Figure S7, which is particularly relevant with a large size difference between the cores.

Another destabilization mechanism observed for the coacervate DE droplets is the "escape" of the dilute core by coalescence with the surrounding continuous phase. This process is shown in Figure 7c and associated side-view schematic for a droplet settled on the glass slide, and in ESI Video 2. Core escape is enabled by the buoyancy of the dilute core, which has a lower density than the coacervate shell. Additionally, the core's coalescence with the surrounding dilute phase also confirms that the shell maintains liquid-like rheology. Nevertheless, it takes several seconds for the core to escape, due to the high viscosity of the dense, slow-flowing coacervate shell. This suggests that the large viscosity contrast between the dense shell and dilute core also hinders the drainage of the shell as the buoyant core rises toward the outer surface of the DE droplet, and thus acts to stabilize the core-shell structure.

Critically, the core escape confirms that these core-shell droplet structures are not at equilibrium with respect to their interfacial behavior. The existence of equilibrated vacuoles in coacervate *bulk* material has been proposed for other systems. For example, Alshareedah et al. argued that formation of vacuoles in coacervate droplets is a reversible "phase transition", since they form when flowing RNA at high concentration over preformed coacervate droplets and disappear upon the addition of RNase-A.[23] However, the time scale for dilute core's disappearance observed therein matches quite well to the time scale for core escape we observe in Figure 7c, namely within seconds once it begins. Our observations suggest that the reversibility of vacuole formation may also be explained by core escape rather than, or in addition to, core dissolution or thermodynamic considerations. Regardless, exploring techniques to control inner-phase escape dynamics—and coacervate DE stability more generally—presents a compelling avenue for further research.

Finally, we observed an unusual mechanism for inner-phase escape from particular double-emulsion droplets with very thin shells − i.e., when the radius of the hollow core (r_{core}) is very similar to the outer radius of the coacervate shell (r_{drop}). This mechanism is depicted in the micrographs in Figure 8a and associated schematic in Figure 8b, as well as in ESI Video 3. Thin-shelled droplets ($r_{drop} \sim 30+ \mu m$) experience large shear rates during core escape, since the characteristic shear rate in the shell scales inversely with shell thickness. In this case, viscoelastic effects can arrest the core escape, resulting in formation of a new, smaller core-shell droplet with a thicker shell and a portion of the former core. The behavior of the shell during the rupture of these thin-shelled coacervate droplets is reminiscent of the recently discovered "flowering" mechanical instability exhibited by bursting bubbles with viscoelasticity in the liquid film,[51] emphasizing the role of the coacervate shell's viscoelasticity (in addition to its large viscosity) in stabilizing the core-shell droplet morphology.

To summarize, we postulate that a *high viscosity contrast* between the dense coacervate shell and the dilute core, as well as *viscoelasticity* of the coacervate shell account for the metastability of the core-shell structures once they form. The high viscosity of the dense phase prevents the dilute cores from moving quickly within the coacervate shell, which slows coalescence of trapped dilute cores with either themselves or with the surrounding dilute phase. In addition, the viscoelastic nature of the coacervate shell can cause retention of a core as it attempts to recoalesce with the surrounding dilute phase due to the coacervate shell's elasticity, especially when the shell is thin relative to its radius. This additionally helps to stabilize the core-shell structure of the double emulsion once it forms.

Since the viscosity of the PAA/PAH dense coacervate phase is lower at high salt concentration,[35,43] this reasoning is consistent with a greater prevalence of DE vs. SE droplets at 1 M vs. 3 M NaCl presented in the "Composition" subsection above. It also explains the greater difference in DE prevalence between low and high salt concentration with excess polycation (relative to excess polyanion). According to theoretical predictions by Aponte-Rivera and Rubenstein,[52] the viscosity contributions of both polycations and polyanions to an unentangled coacervate at high salt are obtained from their respective viscosity in pure solution with concentration similar to that in the coacervate. At equilibrium, under the same degree of polycation excess, the volume fraction of polymer in the PAA/PAH dense phase exceeds the volume fraction under the same degree of polyanion excess at all salt concentrations.[36] Therefore, we expect a greater viscosity of the coacervate under polycation excess, consistent with the greater propensity to form coacervates at PAA:PAH < 1 as observed in Figure 4 herein. Furthermore, the difference in dense phase volume fraction between low and high NaCl is more pronounced under PAH excess,[36] consistent with the greater difference in observed DE between 1 and 3 M NaCl under polycation excess illustrated in Figure S4.

We note that these mechanisms of surfactant-free stabilization are likely general across chemistries of coacervating systems. Another study of vacuolated coacervates have shown

https://doi.org/10.1021/acs.langmuir.4c04201
Langmuir 2025, 41, 8510−8523

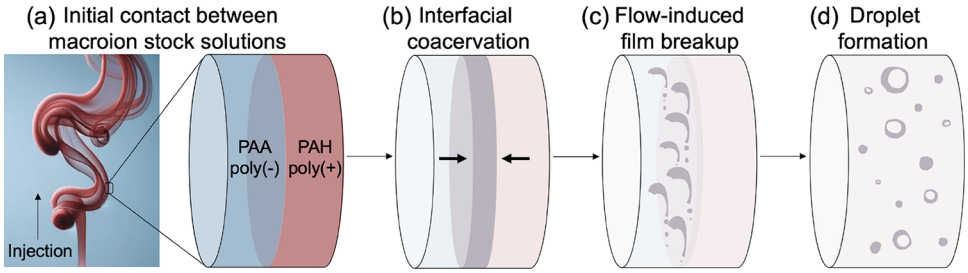

Figure 9. Steps of the proposed mechanism for DE formation during coacervate phase separation. (a) Concept schematic depicting injection of polycation solution (red) into static polyanion solution (blue) (generated by ChatGPT4), and indicating a fluid volume element at the interface; and detail of the fluid element at the interface during initial mixing of the solutions. (b) Coacervate phase separation occurs at the interface (purple), depleting the polycation and polyanion from their respective phases in the directions of the arrows. (c) As the interfacial coacervate forms, recirculating eddys formed by the laminar flow of one stock solution into the other under confinement cause breakup of the interfacial film, as denoted by the sheets of phase-separating coacervate (purple). (d) As result of this process, dilute cores are trapped in some droplets during break up, while others remain single emulsion droplets. A mixture of DE and SE structures is common in many of the conditions in this work.

that the dense phase has high viscosity or even solid-like properties, evidenced by minimal recovery of the fluorescence after photobleaching,[17] which also suggests a high viscosity contrast with water and a strong elastic component. We provide further argument and evidence for the role of a high viscosity contrast in the formation and stabilization of the coacervate DE emulsion structure in the "Composition" subsection above.

Formation Mechanism. A number of studies have proposed that a pre-existing coacervate emulsion is a prerequisite to form core-shell coacervate structures. For example, Sakakibara et al. reported that the presence of a preformed off-stoichiometric complex coacervate was crucial for the formation of multiphase coacervate droplets containing "vacuoles", which only form upon addition of another protein to the system.[24] In different works, vacuoles were formed in pre-existing coacervates due to changes in system parameters such as heating[17−20] or cooling,[21] RNA[21,22] or protein[24] addition, pH change,[17] or a multistep processes analogous to layer-by-layer assembly.[53] Other reports attribute vacuole formation to mechanical or field-driven effects such as solidification of the dense phase,[21] application of external forces,[15,16] or chemical activity.[54] Such studies point to a mechanism whereby phase instability of existing coacervate droplets leads to the nucleation of a vacuole-like core.

We can summarize these previous studies as involving cases where vacuole formation occurs due to phase instability of a pre-existing condensate phase—either due to re-equilibration upon a change of thermodynamic state, or due to slow equilibration or out-of-equilibrium arrest of an evolving coacervate emulsion.[21] Further evidence for this mechanism in such systems is that vacuoles in the coacervate droplets typically formed slowly over the course of 10s of minutes. This slow response is likely due to the high viscosity and viscoelastic character of the coacervate, which, as mentioned above, helps resist the re-equilibration and enable the double emulsion's metastability despite a lack of interfacial stabilization.

Conversely, we do not find that any such many-phase equilibria are necessary to form vacuoles or hollow core-shell condensates in the polyelectrolyte complex coacervate-forming system we study. Herein, DE droplets form equally well if not more abundantly at stoichiometric mixing conditions as compared to conditions that are highly nonstoichiometric. In addition, the DEs form as part of the mixing process, without delay, and with greater propensity when the components are mixed slowly (i.e., with minimal shear forces). This suggests a different mechanism that is related to the coupling of initial phase instability that creates droplets to transport effects, and is therefore distinct from the other mechanisms described previously. We note similarities between the processes and structures we observe to those reported recently by Bui et al.,[55] in which a solution of alginate (polyanion) was slowly dripped into polylysine (polycation) solution. Accordingly, coacervation occurred at the spherically shaped interface between the two solutions, as shown via high-speed imaging. This process results in mm-scale droplets with a coacervate shell forming in 10s of seconds to minutes. A similar approach has been used by Han et al., who used NICE to generate coacervate shells at the interface of dispersed droplets in a PEG/dextran system wherein one phase contains polyanion and the other polycation;[56] and by Lapitsky et al. via dripping a polycation into a solution of anionic surfactant.[57,58] The previous examples all involve diffusion-controlled interfacial coacervation processes.[59] Lapitsky et al. found that larger drops (~2000 vs. ~200 μm, both significantly larger than those studied herein) favor hollow capsule formation, since the amount of solvent required to form regular single-phase droplets increases dramatically with size. In addition, they predicted that surfactants that strongly bind to the polyanion favor hollow morphologies because fast complexation hinders surfactant penetration into the droplet and limits complexation to only a shell layer.[58]

The present work constitutes an extension of these previously reported phenomena to a situation involving stronger (though still gentle) mixing flows, in which the core-shell droplets appear to form spontaneously without being templated by a spherical interface between the mixing streams. We postulate that such DE droplets form due to the fast dynamics of the phase separation at the interface between the solutions as they mix, combined with formation of gentle eddys (in this case due to laminar recirculating flows that form in confined laminar injection[44]) during the injection process that aid the breakup of the transient sheets of interfacial coacervate film and roll them into hollow core-shell droplets as the phase separation proceeds, as illustrated in Figure 9.

Generally, formation of core-shell structures is more favored at a greater salt difference between the mixed solutions. As mentioned previously, there is a strong salt dependence on both the PAA/PAH phase diagram and rheology,[35] in addition to rates of diffusive mass transport. A larger salt gradient facilitates faster interdiffusion (due to electroosmotic effects) and therefore faster phase separation (i.e., faster coacervate

https://doi.org/10.1021/acs.langmuir.4c04201
Langmuir 2025, 41, 8510−8523

formation). This reasoning is consistent with the aforementioned findings by Lapitsky for the polyelectrolyte−surfactant droplet system.[58] Additionally, since the solubility limit of NaCl is 5.4 M at 25 °C,[60] salt differences of 2.5 M correspond to a significant viscosity contrast between the two mixed solutions, which also affects transport. However, we observe only weak effects on core-shell formation as the salt gradient is varied, likely because coacervate phase separation is extremely fast. Stopped-flow mixing experiments have shown that coacervates initially form due to spontaneous charge neutralization immediately after mixing, which occurs within a dead time of 2.5−6 ms.[61,62] This may explain why only larger changes in mass transport—such as affecting advection through large differences in injection rate—seem to have more significant effects on the formation of DEs.

It is important to note that the use of jetting flows (e.g., the injection used here) appears to be important to DE formation, since no DE formation was previously observed in the same mixed polyelectrolyte system during microfluidic Y-junction mixing—which lacks vorticity—even at very slow flow rates ($Re < 1$).[32] For this reason, we propose that the relative frequency and strength of the laminar recirculating Eddys relative to the rate of phase separation controls the formation of *double emulsion* coacervate droplets. Regardless, the presence of recirculating flows (i.e., vorticity during mixing) is not necessarily required for droplet breakup in coacervates in general, given the often low (<10%) volume fraction of the polyelectrolyte-dense coacervate phase. In the context of our proposed mechanism, the mixing flow must be slow enough to allow a large enough contiguous area of interfacial coacervation so that a coacervate sheet can be "rolled" into a dilute-core droplet during the phase separation process. Slower injection rates correspond to gentler mixing conditions that may result in slower film breakup than for finer-scale mixing, thus favoring DE formation. Mass transport rates are also decreased at slower injection conditions, which additionally favors DE formation according to Lapitsky et al. as described above.[58] To summarize, we postulate that slow yet tortuous mixing assists DE formation by (1) slowing the advective mass transport relative to the phase separation, in the context of (2) a flow with laminar recirculating eddys. Further work is required to confirm the exact flow patterns required to form core-shell droplets, as well as the relative contribution of each of these two factors to the observed core-shell formation.

Perhaps the uncommon nature of the mixing conditions employed in this study has led to the perception of the core-shell coacervate droplet structure as rare, uncommon, or system-dependent. Instead, we suspect that the mechanisms described herein may apply to other similar coacervating or liquid−liquid phase separating systems. The proposed DE formation mechanism, though based on specific observations of the PAA/PAH chemistry, is not unique to the specific chemistry or molecular-level details like local chain structure. Several key literature observations support that core-shell coacervate droplet formation from a single dense phase is not particular to the specific chemistry and compositions tested herein. A prior work by Li et al. clearly shows numerous PAA/PAH core-shell droplets above 10 M urea and pH 3 in their Figure 5c micrographs, though the droplet structure is not mentioned in the work.[39] In addition, a prior work by Schmitt et al. on the β-lactoglobulin/acacia gum coacervating system finds a vacuolated or "porous" bulk coacervate phase in Figures 1 and 2 therein, though it is mentioned that "no physicochemical perturbation was applied to [the] system."[63] Though these may be formed from a mechanism of relaxation after flow-induced aggregation as elucidated in our prior work[32] since these porous structures coexist with droplet aggregates in Figure 1 therein, a second paper by Sanchez et al. on the β-lactoglobulin/acacia gum observed the presence of "vesicular and unstable multivesicular coacervate" droplets "a few seconds after mixing" the components.[64] Together, these observations suggest that careful tuning of the mixing parameters, path, and composition could also enable preferential formation of core-shell droplets in the β-lactoglobulin/acacia gum coacervate chemistry by the same mechanism described herein. Overall, we posit that the underlying principles of spontaneous core-shell formation during liquid−liquid phase separation (LLPS) posited herein—namely, coacervate phase behavior, phase separation dynamics, and significant viscosity contrast—could be applied to many other complex-coacervating systems, and even potentially some uncharged LLPS systems, though confirming the mechanism's generality requires extensive experimental evidence that falls outside the scope of the present study.

As an additional consideration, our proposed formation mechanism is consistent with the existence of a lower bound for core-shell size, determined by the thickness of the interfacial coacervate as it is rolled into core-shell droplets. Prior work that observed the formation of core-shell droplets in a chemically fuelled coacervate system found that these nonequilibrium droplets must exceed 3.3 μm in size to stabilize the internal dilute core.[54] While herein we did not observe a lower boundary to the size of DE droplets in this work beyond the resolution of our microscope to multiple layers of a droplet shell (100s of nm), future work that tests for a threshold size for DE droplets formed by the methods used herein would further support the proposed mechanism.

CONCLUSIONS

This work revealed the formation of core-shell or "double emulsion" (DE) coacervates in the two-polyelectrolyte PAA/PAH system. These DE droplets exhibit a dense coacervate shell and dilute vacuole core and are stabilized at the micron scale or larger without surfactants or oily additives. The formation and stability of these hollow DE coacervates depend critically on the composition and processing route.

To assess the formation propensity of the core-shell morphology, we utilized automated microscopy and machine learning (ML) analysis. Our image classification ML model excelled in identifying DE droplets and single-emulsion (SE) droplets (93% and 98% accuracy, respectively). We find that the core-shell morphology readily forms across a wide range of compositions during complex coacervation. The results revealed a preference for DE formation near the 1:1 mixing condition under both low (1 M) and high (3 M) salt conditions. DE formation increased with PAH excess, as did the total number of droplets formed. The general propensity for DE formation across all PAA:PAH ratios was enhanced at low salt, suggesting a fundamental role of salt in core-shell structure stabilization. In particular, decreased salt results in an increase in the coacervate viscosity, which we conclude helps to stabilize the coacervate emulsion's core-shell structure without the surfactant blends required for the stabilization of an analogous water-in-oil-in-water (W/O/W) multiple emulsion system.

https://doi.org/10.1021/acs.langmuir.4c04201
Langmuir 2025, 41, 8510−8523

Additionally, unlike W/O/W emulsion systems—where mixing at low shear rates may eliminate the formation of core-shell structures—we find that core-shell coacervate droplets preferentially form under milder flow conditions (slower injection rates), and that sufficiently fast mixing can completely suppress DE formation. We propose a formation mechanism that relies on carefully tuning the relative rates of phase separation, flow and mass transport in the presence of flows with sufficient vorticity. Specifically, the mass transport must be slow enough relative to the phase separation process that—at a low intensity of injection-based mixing—recirculating eddys form which break up the macroion film into droplets during its formation. A mixture of SE and DE droplets result from this mechanism. Our prior work found no DE droplets using slow mixing in microfluidics,[32] suggesting that the vorticity generated by the injection mixing is an important factor in formation of the core-shell droplets herein. In addition, phase separation dynamics are faster at 1:1 mixing[65] where core-shell droplet formation is favored relative to single-phase droplet formation compared to nonstoichiometric mixing.

Broadly, the DE formation mechanism suggests that continuum effects are more important to their formation than the precise details of the molecular design. This is consistent with emulsion design methods used in oil-water systems, which typically utilize nonequilibrium kinetic approaches to modulate the droplet structure.[5,31] Our approach stands in contrast with prior methods for making substructured coacervate droplets, which require thermodynamic control either through the use of a two-phase templating emulsion[28,29] or through a judicious selection of multiple coexistent dense phases.[13] Our method represents a facile, scalable approach to generate hollow coacervate droplets spontaneously, providing an orthogonal approach to molecular-level engineering.

■ ASSOCIATED CONTENT

Supporting Information

The Supporting Information is available free of charge at https://pubs.acs.org/doi/10.1021/acs.langmuir.4c04201.

ESI document including phase behavior; core and shell fits; image classification model training and evaluation, with example training data, confusion matrices, and other performance quantification; and supplemental data for the salt difference, concentration gradient, and injection rate experiments (PDF)

Core and shell coalescence (AVI)

Inner-phase escape (AVI)

Inner-phase escape from a large droplet (AVI)

■ AUTHOR INFORMATION

Corresponding Author

Matthew E. Helgeson − *Materials Research Laboratory and Department of Chemical Engineering, University of California, Santa Barbara, California 93106-9010, United States;* orcid.org/0000-0001-9384-4023; Phone: +1(805)893-3372; Email: helgeson@ucsb.edu

Authors

Chelsea E. R. Edwards − *Materials Research Laboratory and Department of Chemical Engineering, University of California, Santa Barbara, California 93106-9010, United States;* orcid.org/0000-0003-1540-7594

Hongyi Zhang − *Materials Research Laboratory, University of California, Santa Barbara, California 93106-9010, United States*

Ginny Wang − *Materials Research Laboratory, University of California, Santa Barbara, California 93106-9010, United States*

Complete contact information is available at: https://pubs.acs.org/10.1021/acs.langmuir.4c04201

Notes

The authors declare no competing financial interest.

■ ACKNOWLEDGMENTS

This work was supported by the National Science Foundation Materials Research Science and Engineering Center at UC Santa Barbara (DMR 2308708, IRG-2). CERE was supported in part by the Department of Defense (DoD) through the National Defense Science and Engineering (NDSEG) fellowship. The authors acknowledge the use of the high-throughput characterization facility at the NSF BioPACIFIC MIP at UC Santa Barbara via the Axio Observer 7 microscope. Finally, the authors thank Prof. Megan Valentine for their helpful feedback on buckling-like behavior of the shell; and Prof. Omar Saleh and Prof. Glenn Fredrickson for discussions about the double emulsion formation mechanism.

■ REFERENCES

(1) Tadros, T. F. *Formulations in Cosmetic and Personal Care*; De Gruyter: Berlin, Boston, 2016; Chapter 11, pp 217−230.

(2) Schmitt, C.; Turgeon, S. L. Protein/Polysaccharide Complexes and Coacervates in Food Systems. *Adv. Colloid Interface Sci.* **2011**, *167*, 63−70.

(3) Brangwynne, C. P.; Eckmann, C. R.; Courson, D. S.; Rybarska, A.; Hoege, C.; Gharakhani, J.; Jülicher, F.; Hyman, A. A. Germline P Granules are Liquid Droplets that Localize by Controlled Dissolution/Condensation. *Science* **2009**, *324*, 1729−1732.

(4) Lyon, A. S.; Peeples, W. B.; Rosen, M. K. A Framework for Understanding the Functions of Biomolecular Condensates Across Scales. *Nat. Rev. Mol. Cell Biol.* **2021**, *22*, 215−235.

(5) Sheth, T.; Seshadri, S.; Prileszky, T.; Helgeson, M. E. Multiple Nanoemulsions. *Nat. Rev. Mater.* **2020**, *5*, 214−228.

(6) Blocher McTigue, W. C.; Perry, S. L. Protein Encapsulation Using Complex Coacervates: What Nature Has to Teach Us. *Small* **2020**, *16*, No. 1907671.

(7) Lankalapalli, S.; Kolapalli, V. R. M. Polyelectrolyte Complexes: A Review of Their Applicability in Drug Delivery Technology. *Indian J. Pharm. Sci.* **2009**, *71*, 481.

(8) Gao, S.; Srivastava, S. Comb Polyelectrolytes Stabilize Complex Coacervate Microdroplet Dispersions. *ACS Macro Lett.* **2022**, *11*, 902−909.

(9) Dzieciol, A. J.; Mann, S. Designs for Life: Protocell Models in the Laboratory. *Chem. Soc. Rev.* **2012**, *41*, 79−85.

(10) Feric, M.; Vaidya, N.; Harmon, T. S.; Mitrea, D. M.; Zhu, L.; Richardson, T. M.; Kriwacki, R. W.; Pappu, R. V.; Brangwynne, C. P. Coexisting Liquid Phases Underlie Nucleolar Subcompartments. *Cell* **2016**, *165*, 1686−1697.

(11) Wan, G.; Fields, B. D.; Spracklin, G.; Shukla, A.; Phillips, C. M.; Kennedy, S. Spatiotemporal Regulation of Liquid-Like Condensates in Epigenetic Inheritance. *Nature* **2018**, *557*, 679−683.

(12) Chen, Y.; Yuan, M.; Zhang, Y.; Liu, S.; Yang, X.; Wang, K.; Liu, J. Construction of Coacervate-in-Coacervate Multi-Compartment Protocells for Spatial Organization of Enzymatic Reactions. *Chem. Sci.* **2020**, *11*, 8617−8625.

(13) Lu, T.; Spruijt, E. Multiphase Complex Coacervate Droplets. *J. Am. Chem. Soc.* **2020**, *142*, 2905−2914.
(14) Schijven, L. M.; Saggiomo, V.; Velders, A. H.; Bitter, J. H.; Nikiforidis, C. V. On the Influence of Protein Aggregate Sizes for the Formation of Solid and Hollow Protein Microparticles. *J. Colloid Interface Sci.* **2023**, *631*, 181−190.
(15) Yin, Y.; Niu, L.; Zhu, X.; Zhao, M.; Zhang, Z.; Mann, S.; Liang, D. Non-Equilibrium Behaviour in Coacervate-Based Protocells under Electric-Field-Induced Excitation. *Nat. Commun.* **2016**, *7*, 10658.
(16) Matsumoto, M.; Asoh, T.-A.; Shoji, T.; Tsuboi, Y. Formation of Single Double-Layered Coacervate of Poly (N, N-diethylacrylamide) in Water by a Laser Tweezer. *Langmuir* **2021**, *37*, 2874−2883.
(17) Chen, N.; Zhao, Z.; Wang, Y.; Dimova, R. Resolving the Mechanisms of Soy Glycinin Self-Coacervation and Hollow-Condensate Formation. *ACS Macro Lett.* **2020**, *9*, 1844−1852.
(18) Chen, N.; Zhao, M.; Nicolai, T.; Chassenieux, C. Exploiting Salt Induced Microphase Separation to Form Soy Protein Microcapsules or Microgels in Aqueous Solution. *Biomacromolecules* **2017**, *18*, 2064−2072.
(19) Cochereau, R.; Nicolai, T.; Chassenieux, C.; Silva, J. V. Mechanism of the Spontaneous Formation of Plant Protein Microcapsules in Aqueous Solution. *Colloids Surf., A* **2019**, *562*, 213−219.
(20) Zhao, H.; Zhou, X.; Wang, J.; Ma, X.; Guo, M.; Liu, D. Heat-Induced Hollow Microcapsule Formation using Fava Bean Legumin. *Food Hydrocolloids* **2021**, *112*, No. 106207.
(21) Erkamp, N. A.; Sneideris, T.; Ausserwöger, H.; Qian, D.; Qamar, S.; Nixon-Abell, J.; St George-Hyslop, P.; Schmit, J. D.; Weitz, D. A.; Knowles, T. P. Spatially Non-Uniform Condensates Emerge from Dynamically Arrested Phase Separation. *Nat. Commun.* **2023**, *14*, 684.
(22) Banerjee, P. R.; Milin, A. N.; Moosa, M. M.; Onuchic, P. L.; Deniz, A. A. Reentrant Phase Rransition Drives Dynamic Substructure Formation in Ribonucleoprotein Droplets. *Angew. Chem.* **2017**, *129*, 11512−11517.
(23) Alshareedah, I.; Moosa, M. M.; Raju, M.; Potoyan, D. A.; Banerjee, P. R. Phase Transition of RNA-Protein Complexes into Ordered Hollow Condensates. *Proc. Natl. Acad. Sci. U. S. A.* **2020**, *117*, 15650−15658.
(24) Sakakibara, N.; Ura, T.; Mikawa, T.; Sugai, H.; Shiraki, K. Transient Formation of Multi-Phase Droplets Caused by the Addition of a Folded Protein into Complex Coacervates with an Oppositely Charged Surface Relative to the Protein. *Soft Matter* **2023**, *19*, 4642−4650.
(25) Choi, H.; Hong, Y.; Najafi, S.; Kim, S. Y.; Shea, J.-E.; Hwang, D. S.; Choi, Y. S. Spontaneous Transition of Spherical Coacervate to Vesicle-Like Compartment. *Adv. Sci.* **2024**, *11*, No. 2305978.
(26) Reisch, A.; Tirado, P.; Roger, E.; Boulmedais, F.; Collin, D.; Voegel, J.-C.; Frisch, B.; Schaaf, P.; Schlenoff, J. B. Compact Saloplastic Poly(Acrylic Acid)/Poly(Allylamine) Complexes: Kinetic Control Over Composition, Microstructure, and Mechanical Properties. *Adv. Funct. Mater.* **2013**, *23*, 673−682.
(27) Zhao, P.; Guo, J.; Jiang, T.; Xu, X.; Chen, S.; Li, Z.; Xu, J.; Li, G.; Bian, L. Vacuolated Coacervate Mediates the Bimodal Release Kinetics of Diverse Macromolecular Drugs in vivo. *Mater. Today* **2023**, *66*, 26−35.
(28) Zhang, L.; Cai, L.-H.; Lienemann, P. S.; Rossow, T.; Polenz, I.; Vallmajo-Martin, Q.; Ehrbar, M.; Na, H.; Mooney, D. J.; Weitz, D. A. One-Step Microfluidic Fabrication of Polyelectrolyte Microcapsules in Aqueous Conditions for Protein Release. *Angew. Chem.* **2016**, *128*, 13668−13672.
(29) Kim, M.; Yeo, S. J.; Highley, C. B.; Burdick, J. A.; Yoo, P. J.; Doh, J.; Lee, D. One-Step Generation of Multifunctional Polyelectrolyte Microcapsules via Nanoscale Interfacial Complexation in Emulsion (NICE). *ACS Nano* **2015**, *9*, 8269−8278.
(30) Hann, S. D.; Stebe, K. J.; Lee, D. AWE-somes: All Water Emulsion Bodies with Permeable Shells and Selective Compartments. *ACS Appl. Mater. Interfaces* **2017**, *9*, 25023−25028.
(31) Saether, O.; Sjoblom, J.; Dukhin, S. S. *Food Emulsions*; Marcel Dekker: New York, 2004; Vol. *4*, Chapter 5.
(32) Edwards, C. E. R.; Lakkis, K. L.; Luo, Y.; Helgeson, M. E. Coacervate or Precipitate? Formation of Non-Equilibrium Microstructures in Coacervate Emulsions. *Soft Matter* **2023**, *19*, 8849.
(33) Magana, J. R.; Sproncken, C. C.; Voets, I. K. On Complex Coacervate Core Micelles: Structure-Function Perspectives. *Polymers* **2020**, *12*, 1953.
(34) Ji, Y.; Lin, Y.; Qiao, Y. Plant cell-inspired membranization of coacervate protocells with a structured polysaccharide layer. *J. Am. Chem. Soc.* **2023**, *145*, 12576−12585.
(35) Luo, Y.; Gu, M.; Edwards, C. E.; Valentine, M. T.; Helgeson, M. E. High-Throughput Microscopy to Determine Morphology, Microrheology, and Phase Boundaries Applied to Phase Separating Coacervates. *Soft Matter* **2022**, *18*, 3063−3075.
(36) Nguyen, M.; Sherck, N.; Shen, K.; Edwards, C. E.; Yoo, B.; Kohler, S.; Speros, J. C.; Helgeson, M. E.; Delaney, K. T.; Shell, M. S.; Fredrickson, G. H. Predicting Polyelectrolyte Coacervation from a Molecularly Informed Field-Theoretic Model. *Macromolecules* **2022**, *55*, 9868−9879.
(37) Crocker, J. C.; Grier, D. G. Methods of Digital Video Microscopy for Colloidal Studies. *J. Colloid Interface Sci.* **1996**, *179*, 298−310.
(38) Liu, Z.; Jin, L.; Chen, J.; Fang, Q.; Ablameyko, S.; Yin, Z.; Xu, Y. A Survey on Applications of Deep Learning in Microscopy Image Analysis. *Comput. Biol. Med.* **2021**, *134*, No. 104523.
(39) Li, L.; Srivastava, S.; Meng, S.; Ting, J. M.; Tirrell, M. V. Effects of non-electrostatic intermolecular interactions on the phase behavior of pH-sensitive polyelectrolyte complexes. *Macromolecules* **2020**, *53*, 7835−7844.
(40) Tang, T. D.; Hak, C. R. C.; Thompson, A. J.; Kuimova, M. K.; Williams, D.; Perriman, A. W.; Mann, S. Fatty Acid Membrane Assembly on Coacervate Microdroplets as a Step Towards a Hybrid Protocell Model. *Nat. Chem.* **2014**, *6*, 527−533.
(41) Zhang, P.; Shen, K.; Alsaifi, N. M.; Wang, Z.-G. Salt Partitioning in Complex Coacervation of Symmetric Polyelectrolytes. *Macromolecules* **2018**, *51*, 5586−5593.
(42) Lou, J.; Friedowitz, S.; Qin, J.; Xia, Y. Tunable Coacervation of Well-Defined Homologous Polyanions and Polycations by Local Polarity. *ACS Cent. Sci.* **2019**, *5*, 549−557.
(43) Syed, V. M.; Srivastava, S. Time−Ionic Strength Superposition: A Unified Description of Chain Relaxation Dynamics in Polyelectrolyte Complexes. *ACS Macro Lett.* **2020**, *9*, 1067−1073.
(44) Sarma, A.; Sundararajan, T.; Ramjee, V. Numerical Simulation of Confined Laminar Jet Flows. *Int. J. Numer. Methods Fluids* **2000**, *33*, 609−626.
(45) Quezada, G. R.; Toro, N.; Saavedra, J.; Robles, P.; Salazar, I.; Navarra, A.; Jeldres, R. I. Molecular Dynamics Study of the Conformation, Ion Adsorption, Diffusion, and Water Structure of Soluble Polymers in Saline Solutions. *Polymers* **2021**, *13*, 3550.
(46) Cakmak, F. P.; Grigas, A. T.; Keating, C. D. Lipid Vesicle-Coated Complex Coacervates. *Langmuir* **2019**, *35*, 7830−7840.
(47) Martin, N.; Li, M.; Mann, S. Selective Uptake and Refolding of Globular Proteins in Coacervate Microdroplets. *Langmuir* **2016**, *32*, 5881−5889.
(48) Deshpande, S.; Brandenburg, F.; Lau, A.; Last, M. G.; Spoelstra, W. K.; Reese, L.; Wunnava, S.; Dogterom, M.; Dekker, C. Spatiotemporal control of coacervate formation within liposomes. *Nat. Commun.* **2019**, *10*, 1800.
(49) Bungenberg de Jong, H. G. Crystallisation-coacervation-flocculation. *Colloid Sci.* **1949**, *2*, 232−258.
(50) Smokers, I. B.; Visser, B. S.; Slootbeek, A. D.; Huck, W. T.; Spruijt, E. How Droplets Can Accelerate Reactions Coacervate Protocells as Catalytic Microcompartments. *Acc. Chem. Res.* **2024**, *57*, 1885−1895.
(51) Tammaro, D.; Chandran Suja, V.; Kannan, A.; Gala, L. D.; Di Maio, E.; Fuller, G. G.; Maffettone, P. L. Flowering in Bursting Bubbles with Viscoelastic Interfaces. *Proc. Natl. Acad. Sci. U. S. A.* **2021**, *118*, No. e2105058118.

https://doi.org/10.1021/acs.langmuir.4c04201
Langmuir 2025, 41, 8510−8523

(52) Aponte-Rivera, C.; Rubinstein, M. Dynamic coupling in unentangled liquid coacervates formed by oppositely charged polyelectrolytes. *Macromolecules* **2021**, *54*, 1783−1800.
(53) Liu, W.; Samanta, A.; Deng, J.; Akintayo, C. O.; Walther, A. Mechanistic Insights into the Phase Separation Behavior and Pathway-Directed Information Exchange in all-DNA Droplets. *Angew. Chem.* **2022**, *134*, No. e202208951.
(54) Bergmann, A. M.; Bauermann, J.; Bartolucci, G.; Donau, C.; Stasi, M.; Holtmannspötter, A.-L.; Jülicher, F.; Weber, C. A.; Boekhoven, J. Liquid Spherical Shells are a Non-Equilibrium Steady State of Active Droplets. *Nat. Commun.* **2023**, *14*, 6552.
(55) Bui, T. V. A.; Kim, J.-J.; Huang, X.; Pu, A.; Li, X.; Hong, S. B.; Choi, Y.-J.; Kim, H.-W.; Yao, X.; Park, H.-J.; et al. Core−Shell Droplet-Based Angiogenic Patches for the Treatment of Ischemic Diseases: Ultrafast Processability, Physical Tunability, and Controlled Delivery of an Angiogenic Cocktail. *ACS Appl. Mater. Interfaces* **2023**, *15*, 50693.
(56) Hann, S. D.; Lee, D.; Stebe, K. J. Tuning Interfacial Complexation in Aqueous Two-Phase Systems with Polyelectrolytes and Nanoparticles for Compound All Water Emulsion Bodies (AWE-somes). *Phys. Chem. Chem. Phys.* **2017**, *19*, 23825−23831.
(57) Lapitsky, Y.; Kaler, E. W. Formation of Surfactant and Polyelectrolyte Gel Particles in Aqueous Solutions. *Colloids Surf., A* **2004**, *250*, 179−187.
(58) Lapitsky, Y.; Kaler, E. W. Formation and structural control of surfactant and polyelectrolyte gels. *Colloids Surf., A* **2006**, *282*, 118−128.
(59) Huang, X.; Tian, L.; Wang, Z.; Zhang, J.; Chan, Y. S.; Cheng, S. H.; Yao, X. Bioinspired Robust All-Aqueous Droplet via Diffusion-Controlled Interfacial Coacervation. *Adv. Funct. Mater.* **2020**, *30*, No. 2004166.
(60) Perry, D. L. *Handbook of Inorganic Compounds*; CRC Press, 2016.
(61) Amann, M.; Diget, J. S.; Lyngsø, J.; Pedersen, J. S.; Narayanan, T.; Lund, R. Kinetic Pathways for Polyelectrolyte Coacervate Micelle Formation Revealed by Time-Resolved Synchrotron SAXS. *Macromolecules* **2019**, *52*, 8227−8237.
(62) Takahashi, R.; Narayanan, T.; Sato, T. Growth Kinetics of Polyelectrolyte Complexes Formed from Oppositely-Charged Homopolymers Studied by Time-Resolved Ultra-Small-Angle X-ray Scattering. *J. Phys. Chem. Lett.* **2017**, *8*, 737−741.
(63) Schmitt, C.; Sanchez, C.; Lamprecht, A.; Renard, D.; Lehr, C.-M.; de Kruif, C. G.; Hardy, J. Study of β-lactoglobulin/acacia gum complex coacervation by diffusing-wave spectroscopy and confocal scanning laser microscopy. *Colloids Surf., B* **2001**, *20*, 267−280.
(64) Sanchez, C.; Mekhloufi, G.; Schmitt, C.; Renard, D.; Robert, P.; Lehr, C.-M.; Lamprecht, A.; Hardy, J. Self-assembly of β-lactoglobulin and acacia gum in aqueous solvent: structure and phase-ordering kinetics. *Langmuir* **2002**, *18*, 10323−10333.
(65) Chen, S.; Wang, Z.-G. Charge Asymmetry Suppresses Coarsening Dynamics in Polyelectrolyte Complex Coacervation. *Phys. Rev. Lett.* **2023**, *131*, No. 218201.

https://doi.org/10.1021/acs.langmuir.4c04201
Langmuir 2025, 41, 8510−8523